

Galaxy Zoo: building the low-mass end of the red sequence with local
post-starburst galaxies

William C. Keel – University of Alabama
et al.

Deposited 09/21/2018

Citation of published version:

Wong, O. et al. (2012): Galaxy Zoo: building the low-mass end of the red sequence with
local post-starburst galaxies. *Monthly Notices of the Royal Astronomical Society*, 420(2).

DOI: <https://doi.org/10.1111/j.1365-2966.2011.20159.x>



This work is licensed under a [Creative Commons Attribution 4.0 International License](https://creativecommons.org/licenses/by/4.0/)

Published by Oxford University Press on behalf of the Royal Astronomical Society

© 2012 The Author(s)

Galaxy Zoo: building the low-mass end of the red sequence with local post-starburst galaxies[★]

O. I. Wong,^{1,2†} K. Schawinski,^{3,4‡} S. Kaviraj,^{5,6} K. L. Masters,^{7,8} R. C. Nichol,⁷
C. Lintott,^{6,9} W. C. Keel,¹⁰ D. Darg,⁶ S. P. Bamford,¹¹ D. Andreescu,¹² P. Murray,¹³
M. J. Raddick,¹⁴ A. Szalay,¹⁴ D. Thomas⁷ and J. VandenBerg¹⁴

¹CSIRO Astronomy & Space Science, PO Box 76, Epping, NSW 1710, Australia

²Astronomy Department, Yale University, PO Box 208101, New Haven, CT 06520-8101, USA

³Department of Physics, Yale University, New Haven, CT 06511, USA

⁴Yale Center for Astronomy and Astrophysics, Yale University, PO Box 208121, New Haven, CT 06520, USA

⁵Blackett Laboratory, Imperial College London, South Kensington Campus, London SW7 2AZ

⁶Oxford Astrophysics, Department of Physics, University of Oxford, Denys Wilkinson Building, Keble Road, Oxford OX1 3RH

⁷Institute for Cosmology and Gravitation, Dennis Sciama Building, University of Portsmouth, Burnaby Road, Portsmouth PO1 3FX

⁸South East Physics Network, SEPnet (www.sepnet.ac.uk)

⁹Adler Planetarium, 1300 S. Lakeshore Drive, Chicago, IL 60605, USA

¹⁰Department of Physics & Astronomy, University of Alabama, 206 Gallalee Hall, 514 University Boulevard, Tuscaloosa, AL 35487-0234, USA

¹¹Centre for Astronomy & Particle Theory, University of Nottingham, University Park, Nottingham NG7 2RD

¹²LinkLab, 4506 Graystone Avenue, Bronx, NY 10471, USA

¹³Fingerprint Digital Media, 9 Victoria Close, Newtownards BT23 7GY

¹⁴Department of Physics and Astronomy, The Johns Hopkins University, Homewood Campus, Baltimore, MD 21218, USA

Accepted 2011 November 5. Received 2011 November 5; in original form 2011 May 15

ABSTRACT

We present a study of local post-starburst galaxies (PSGs) using the photometric and spectroscopic observations from the Sloan Digital Sky Survey and the results from the Galaxy Zoo project. We find that the majority of our local PSG population have neither early- nor late-type morphologies but occupy a well-defined space within the colour–stellar mass diagram, most notably, the low-mass end of the ‘green valley’ below the transition mass thought to be the mass division between low-mass star-forming galaxies and high-mass passively evolving bulge-dominated galaxies. Our analysis suggests that it is likely that local PSGs will quickly transform into ‘red’, low-mass early-type galaxies as the stellar morphologies of the ‘green’ PSGs largely resemble that of the early-type galaxies within the same mass range. We propose that the current population of PSGs represents a population of galaxies which is rapidly transitioning between the star-forming and the passively evolving phases. Subsequently, these PSGs will contribute towards the build-up of the low-mass end of the ‘red sequence’ once the current population of young stars fade and stars are no longer being formed. These results are consistent with the idea of ‘downsizing’ where the build-up of smaller galaxies occurs at later epochs.

Key words: galaxies: evolution.

1 INTRODUCTION

Current research in galaxy evolution is still largely driven by our lack of understanding of the link between the two main types of

galaxies observed in the sky. Many theories exist to explain the evolution between star-forming (SF), gas-rich spiral galaxies (‘late’ type) and non-star-forming (non-SF), passively evolving spheroidal galaxies (‘early’-type). Since this bimodal nature is highly correlated to the stellar age and star formation history of the individual galaxies, it is likely that we are observing two main stages of galaxy evolution (Strateva et al. 2001; Baldry et al. 2004, 2006; Kauffmann et al. 2004; Drory et al. 2009), and that the transition between these two types occurs relatively quickly (Martin et al. 2007). The colours and brightnesses (as defined by their observed magnitudes) of all galaxies appear to be concentrated within two well-defined

[★]This publication has been made possible by the participation of more than 250 000 volunteers in the Galaxy Zoo project. Their contributions are individually acknowledged at <http://www.galaxyzoo.org/Volunteers.aspx>.

[†]E-mail: ivy.wong@csiro.au

[‡]Einstein Fellow.

colour–magnitude regions. The SF galaxies appear to populate a space dubbed the ‘blue cloud’, and the passively evolving, non-SF galaxies lie in a region called the ‘red sequence’. Recent studies argue that local galaxies must migrate rapidly (within a Gyr) from the ‘blue cloud’ to the ‘red sequence’¹ due to the scarcity of galaxies within the intervening parameter space (occasionally dubbed the ‘green valley’; e.g. Schawinski et al. 2007b). Therefore, valuable insights into galaxy evolution can be obtained by studying galaxies that appear to have intermediate properties and may be in the act of transitioning between the two main galaxy populations.

Post-starburst galaxies (PSGs) or post- quenching galaxies (Yan et al. 2009), such as ‘E+A’ or ‘K+A’ galaxies, are galaxies that appear to have ceased current star formation, but still exhibit the spectral signature of recently formed stars. In E+A galaxies, strong Balmer absorption lines are observed together with α -element signatures such as Mg₅₁₇₅, Fe₅₂₇₀ and Ca_{3934,3468} (Dressler & Gunn 1983, 1992; Couch & Sharples 1987; MacLaren, Ellis & Couch 1988; Newberry, Boroson & Kirshner 1990; Fabricant, McClintock & Bautz 1991; Abraham et al. 1996; Dressler et al. 1999, 2004; Poggianti et al. 1999; Goto et al. 2003; Goto 2004, 2005, 2007). Similar to E+A galaxies, K+A galaxies are PSGs which have a disc-like morphology (Couch et al. 1994; Dressler et al. 1994; Caldwell & Rose 1997; Dressler et al. 1999). Although PSGs such as E+A galaxies are more common at higher redshifts (Tran et al. 2004; Wild et al. 2009), detailed high-resolution studies are only possible with a local population of PSGs since low-redshift observations extend to lower surface brightness limits than that at earlier epochs.

Current studies favour the idea that PSGs are formed via interactions or major mergers (Bekki, Shioya & Couch 2001; Blake et al. 2004; Yamauchi, Yagi & Goto 2008) which trigger bursts of star formation. However, due to the effects of the merger interaction, the gas reservoir (from which stars are formed) is depleted and these PSGs eventually turn into bulge-dominated early-type galaxies once their star formation fades completely (e.g. Yang et al. 2008). Kaviraj et al. (2007) found that the quenching efficiency of star formation in less massive ($<10^{10} M_{\odot}$) and more massive E+A galaxies ($>10^{10} M_{\odot}$) is consistent with supernovae and active galactic nuclei (AGNs) being the main sources of negative feedback, respectively.

Using the Sloan Digital Sky Survey (SDSS), we assemble and analyse one of the largest, and most complete samples, of local PSGs to date. This paper investigates the properties of the local PSGs derived from the visual classifications of the Galaxy Zoo citizen science project (Lintott et al. 2008, 2011).

Section 2 describes our sample selection, and the sample properties are examined in Section 3. A discussion of our results and conclusions can be found in Section 4. The AB magnitude system is used throughout this work.

2 OUR GALAXY SAMPLE

In this paper, we obtain the photometric and spectroscopic data from the SDSS DR7 (York et al. 2000; Abazajian et al. 2009) for all

objects classified as ‘galaxy’ (Strauss et al. 2002). The main galaxy emission-line measurements are determined from the SDSS spectra using the GANDALF IDL tool by Sarzi et al. (2006). To minimize the Malmquist bias, and create a volume- and magnitude-limited (proxy for stellar mass limited) sample of galaxies, we select all the galaxies within $0.02 < z < 0.05$ with $M_{z,\text{Petro}} < -19.5$ mag. We use the z band since the reddest waveband provides the closest proxy to stellar mass. It should be noted that the results of this paper remain unchanged if the i band is used instead. As we aim to study the properties of all galaxies that have ceased star formation recently, we define a PSG to be a galaxy with a recently truncated star formation history (i.e. where the observed H α emission line is weaker than four times the rms level), while still exhibiting strong Balmer absorption lines from recently formed young stars (where the H δ equivalent width is wider than 3 Å). Our strict H α criterion may result in the omission of a few PSGs known to emit weak H α emission, but the effects from the inclusion of a few H α -emitting galaxies do not change any of the results that we present in Section 3.

Studies such as Balogh et al. (1999), Blake et al. (2004) and Goto (2007) select for PSGs at higher redshifts ($0.5 < z < 1.0$) which exhibit very strong A-type stellar populations (where the observed H δ equivalent width is wider than 5 Å). To include as many PSGs as possible into our sample, we imposed a more relaxed H δ equivalent width so we do not bias against galaxies with a low star formation rate (SFR) (which results in weaker Balmer equivalent widths) prior to the cessation of star formation.

The [O II] forbidden lines were not used in the selection criteria because the H α emission line is a more accurate tracer of current star formation in the local Universe. The luminosity of the [O II] emission lines is not directly linked to the ionizing luminosity and the [O II] excitation is sensitive to the abundance and the ionization state of the gas (Kennicutt 1998). Moreover, the [O II]-derived SFRs are sensitive to systematic errors from extinction and variations in the diffused gas fraction (Kennicutt 1998). In starburst galaxies, the excitation of [O II] is much higher in the diffused ionized gas (Hunter & Gallagher 1990; Hunter 1994; Martin 1998), and is able to double the $L[\text{O II}]/\text{SFR}$ ratio in the integrated spectrum (Kennicutt 1992).

Of 47 573 galaxies within our selected volume, we find a total of 80 PSGs. The general properties of our PSGs are listed in Table 1. Fig. 1 shows the SDSS multicolour composite images for 12 random PSGs within our sample. This figure exhibits the variety of morphologies and sizes within our PSG sample.

Using the bootstrap resampling method to approximate the uncertainty, we find that our percentage of PSGs to the total number of galaxies (within our specified volume out to $z \sim 0.05$) is $0.17^{+0.07}_{-0.05}$ per cent. This assumes that the uncertainty in our spectral line measurements is given by the signal-to-noise ratio. This PSG fraction is comparable to that of previous local PSG studies by Goto (2005, 2007) and Kaviraj et al. (2007). It should be noted that we do not find many of the E+A galaxies found by (Goto 2005, 2007, hereafter known as the ‘G05’ sample) from the SDSS DR5 catalogue because we detect strong H α emission in these G05 objects using the SDSS DR7 catalogue. Hence, these E+A galaxies appear to have current, on-going star formation and is inconsistent with our definition of a PSG. Of the overlapping galaxies between our full galaxy sample and that of the G05 sample, we find that our method of using the Balmer absorption line strength finds every galaxy found via its absorption line equivalent width. This is consistent with the fact that there is a good correlation between the line strengths and the equivalent widths for galaxies of similar sizes.

¹ There are a few cases where the evolution of individual galaxies moves from the ‘red sequence’ to the ‘blue cloud’ (e.g. Kannappan, Guie & Baker 2009; Wei et al. 2010). In these cases, passively evolving galaxies have accreted more gas recently and are in the process of regrowing their stellar disc. However, this ‘red to blue’ mode of evolution is very unlikely to apply to our particular study because our PSGs are defined to have no current on-going star formation.

Table 1. General properties of our PSG sample.

SDSS object ID (1)	RA (2)	Dec. (3)	m_r (4)	$u - r$ (5)	EW(H δ) (6)	$S_{\text{[OII]}}$ (7)	$S_{\text{H}\alpha}$ (8)	$\log(M_{\star})$ (9)	f_m (10)	fracDev (11)	Type (12)	Comment
587731513679478898	01:14:47.2	+00:37:55.7	16.75	2.00	3.4	$<7.9 \times 10^{-15}$	–	9.95	0.000	0.595	I	–
587731513681313986	01:31:37.9	+00:48:51.7	16.52	1.37	5.0	$<2.4 \times 10^{-16}$	$<1.3 \times 10^{-17}$	9.69	0.000	0.000	I	–
587731511533961332	01:32:50.2	–00:56:17.6	16.86	2.11	4.7	$<6.4 \times 10^{-15}$	$<1.5 \times 10^{-15}$	10.03	0.000	1.000	I	Blob
587727230522032233	01:37:16.4	–09:29:06.5	16.63	2.25	3.7	$<1.2 \times 10^{-16}$	–	9.96	0.000	0.546	I	Blob
588015510358524013	02:20:38.7	+00:54:09.1	15.15	0.97	4.1	1.5×10^{-13}	$<6.3 \times 10^{-15}$	9.66	0.000	0.240	S	–
587731512082956346	03:23:33.3	–00:26:18.8	14.92	2.04	4.2	–	$<7.3 \times 10^{-14}$	9.99	0.000	0.770	E	–
587731514232996008	03:47:10.2	+01:04:39.9	15.78	1.77	3.9	$<4.8 \times 10^{-16}$	$<4.7 \times 10^{-17}$	9.97	0.000	0.007	I	–
587732053779283987	08:43:20.7	+37:13:27.6	16.24	2.26	3.7	$<5.5 \times 10^{-16}$	$<3.1 \times 10^{-16}$	10.23	0.000	0.926	I	Blob
587744874791370929	09:01:03.8	+13:36:33.3	14.91	0.85	4.0	1.7×10^{-13}	$<1.2 \times 10^{-14}$	9.82	0.188	0.505	I	Disturbed
587745403073855572	09:11:31.1	+12:08:52.1	14.96	2.22	3.3	$<1.0 \times 10^{-14}$	$<2.4 \times 10^{-15}$	10.43	0.047	1.000	I	Disturbed
587745540514119842	09:25:03.2	+13:03:58.0	16.56	2.06	3.0	$<3.5 \times 10^{-14}$	$<2.2 \times 10^{-15}$	9.81	0.000	1.000	I	Blob
588016891707392070	09:29:34.6	+33:47:51.1	15.28	1.22	4.3	1.1×10^{-13}	$<1.6 \times 10^{-14}$	9.70	0.115	0.000	I	Disturbed
587745243626405989	09:45:00.0	+15:27:40.0	15.79	2.10	4.0	$<1.2 \times 10^{-14}$	$<4.2 \times 10^{-15}$	10.25	0.000	0.609	I	Blob
587735044693753946	09:46:29.9	+39:02:19.7	16.72	1.34	3.9	1.9×10^{-13}	$<1.2 \times 10^{-14}$	9.61	0.000	0.620	I	–
587725074458804315	09:49:56.4	–00:13:52.9	13.89	2.36	3.4	$<6.5 \times 10^{-16}$	$<2.7 \times 10^{-16}$	11.35	0.095	1.000	I	Disturbed
588848900973789221	10:04:29.8	+00:41:20.2	16.49	2.06	3.2	$<1.8 \times 10^{-16}$	$<2.1 \times 10^{-16}$	9.93	0.000	0.870	I	Blob
587726032236183669	10:06:50.9	+01:41:34.0	16.94	2.08	5.7	$<2.0 \times 10^{-16}$	–	9.84	0.074	0.613	I	Blob
587738948283334792	10:12:18.9	+36:07:50.0	15.62	1.59	3.3	1.1×10^{-13}	$<1.9 \times 10^{-14}$	9.96	0.000	0.964	I	Blob
587741828579393617	10:21:25.9	+21:32:45.8	16.00	1.90	4.1	–	$<6.2 \times 10^{-16}$	9.91	0.000	0.002	S	–
587733080268931236	10:30:53.7	+51:19:59.6	15.05	1.18	4.2	4.9×10^{-15}	$<8.3 \times 10^{-16}$	10.35	0.031	0.194	S	Asymmetric
587728947978436717	10:42:32.3	–00:41:58.3	15.83	2.07	4.3	$<2.9 \times 10^{-16}$	$<7.5 \times 10^{-16}$	10.10	0.000	0.994	I	Blob
587729386611212446	10:53:05.4	+57:51:54.2	15.60	1.10	3.8	3.7×10^{-16}	$<1.5 \times 10^{-16}$	10.05	0.000	0.054	I	–
587734894357381314	11:00:48.5	+10:31:19.0	16.44	2.23	4.2	$<6.1 \times 10^{-15}$	$<1.6 \times 10^{-15}$	10.12	0.000	0.864	I	Asymmetric
587741489834754106	11:10:33.9	+28:29:33.3	15.73	2.07	4.1	–	$<1.4 \times 10^{-14}$	10.00	0.000	0.985	I	Blob
588848898833842380	11:13:28.0	–00:54:09.5	16.62	2.03	4.9	$<2.5 \times 10^{-14}$	$<3.7 \times 10^{-15}$	9.57	0.000	0.771	I	Blob
587732580982521898	11:19:07.6	+58:03:14.3	14.17	2.16	4.7	1.6×10^{-13}	$<2.9 \times 10^{-14}$	10.74	0.000	1.000	I	Asymmetric
587739405703577638	11:26:53.7	+33:07:09.5	14.86	1.21	4.5	1.3×10^{-13}	$<7.3 \times 10^{-15}$	9.92	0.108	0.190	S	–
587732482746548338	11:35:32.0	+48:56:38.5	15.99	2.19	4.0	$<6.5 \times 10^{-15}$	$<1.3 \times 10^{-15}$	9.76	0.017	0.866	I	Disturbed
587741726574444657	11:36:55.2	+24:53:25.5	14.92	1.73	5.5	1.4×10^{-13}	$<5.0 \times 10^{-11}$	9.98	0.027	0.200	I	Disturbed
587742573224657026	11:43:47.8	+20:21:48.0	15.61	1.83	6.7	$<8.2 \times 10^{-15}$	–	9.56	0.000	0.305	S	Disturbed
588017111833182222	12:21:05.7	+47:58:51.9	16.54	2.18	3.6	$<7.2 \times 10^{-14}$	$<2.2 \times 10^{-15}$	10.02	0.000	0.978	I	–
588017730836561977	12:26:41.6	+08:44:32.2	15.42	2.45	6.5	$<8.9 \times 10^{-13}$	$<4.9 \times 10^{-14}$	10.38	0.000	0.906	I	–
587726033325850747	12:32:18.9	+03:00:09.8	16.82	2.00	3.3	$<6.2 \times 10^{-14}$	–	10.10	0.000	1.000	I	Blob
587725816414142618	12:32:23.3	+66:25:36.6	16.90	2.26	3.1	$<1.0 \times 10^{-16}$	–	9.82	0.032	0.528	I	Blob
587734892220252284	12:37:18.0	+09:32:09.0	14.55	1.89	3.0	$<3.4 \times 10^{-16}$	–	9.84	0.000	0.979	E	–
587739096454332452	12:38:52.8	+36:32:05.7	15.74	2.15	3.7	$<1.2 \times 10^{-16}$	$<1.3 \times 10^{-17}$	10.19	0.000	1.000	E	–
587741602572599308	12:57:17.8	+27:48:39.3	15.40	1.97	3.9	$<1.7 \times 10^{-15}$	$<4.4 \times 10^{-18}$	9.74	0.000	0.211	I	Disturbed
587741722823557134	12:57:21.7	+27:52:49.5	15.23	2.10	3.6	$<5.1 \times 10^{-15}$	$<1.9 \times 10^{-17}$	9.94	0.000	0.873	E	–
587741722286686489	12:57:45.7	+27:25:45.6	15.92	1.94	3.9	$<1.3 \times 10^{-13}$	$<1.1 \times 10^{-14}$	9.56	0.000	0.254	S	–
587741721749881039	12:58:12.0	+27:07:39.5	16.60	2.31	3.5	$<3.0 \times 10^{-14}$	–	10.06	0.000	0.806	S	–
587741722823754043	12:59:39.5	+27:51:16.6	16.57	2.20	4.2	$<3.7 \times 10^{-17}$	$<1.1 \times 10^{-17}$	9.95	0.454	0.343	I	Disturbed
587741722823819345	13:00:10.2	+27:51:50.2	15.85	2.22	3.4	$<2.8 \times 10^{-15}$	–	10.00	0.097	0.357	I	Disturbed
587741722286948519	13:00:29.2	+27:30:53.4	15.53	1.63	8.5	$<1.1 \times 10^{-15}$	$<9.6 \times 10^{-17}$	9.55	0.125	0.224	I	Disturbed
587739719754514434	13:04:22.7	+28:48:38.8	14.33	0.86	4.4	$<2.9 \times 10^{-12}$	$<4.2 \times 10^{-14}$	10.15	0.365	0.643	S	Disturbed
587733195160485975	13:05:25.8	+53:35:30.3	14.29	2.15	4.6	$<4.8 \times 10^{-16}$	$<1.4 \times 10^{-16}$	10.75	0.000	1.000	E	–
587722982822379684	13:17:59.6	–00:17:43.2	13.29	1.22	5.2	$<2.1 \times 10^{-14}$	$<5.1 \times 10^{-14}$	10.44	0.139	0.477	S	Asymmetric
587729773681377291	13:37:44.1	–02:10:27.9	14.61	0.72	3.5	–	$<2.5 \times 10^{-14}$	10.41	0.000	0.338	S	–
587726032797565040	13:50:51.0	+02:19:38.5	15.62	2.11	4.7	$<3.2 \times 10^{-16}$	$<8.7 \times 10^{-17}$	9.97	0.167	1.000	I	Disturbed
587730021178867826	14:18:51.0	+05:28:14.2	15.92	2.09	3.0	$<7.3 \times 10^{-15}$	$<2.6 \times 10^{-15}$	9.90	0.000	0.961	I	Blob
587739827130007710	14:39:08.5	+22:17:42.4	15.42	0.84	4.5	2.0×10^{-14}	$<1.1 \times 10^{-15}$	9.75	0.136	0.000	I	Asymmetric
587739408405626997	14:39:30.4	+30:52:49.1	16.14	1.97	4.2	$<5.0 \times 10^{-14}$	$<1.3 \times 10^{-15}$	9.97	0.153	1.000	I	Bisturbed
587739379916210254	14:54:24.7	+27:39:38.7	16.23	2.04	3.9	$<1.8 \times 10^{-16}$	$<4.2 \times 10^{-17}$	9.98	0.000	1.000	I	Blob
587726032268362094	15:01:24.0	+01:39:25.0	15.90	1.92	3.9	–	$<4.5 \times 10^{-15}$	9.95	0.000	0.682	I	Blob
588017949366157511	15:03:39.4	+35:27:30.5	16.14	0.94	3.9	1.8×10^{-13}	$<6.4 \times 10^{-15}$	9.60	0.000	0.000	I	–
587736975271067720	15:12:04.1	+28:25:14.1	14.26	1.20	4.2	1.3×10^{-15}	$<4.7 \times 10^{-15}$	10.43	0.015	0.772	I	Asymmetric
588017991773978739	15:14:29.9	+07:35:46.8	15.45	1.97	4.4	$<4.7 \times 10^{-14}$	$<5.5 \times 10^{-15}$	10.27	0.000	0.918	I	Blob
587736543098568963	15:21:08.6	+07:37:53.9	16.40	2.05	4.9	$<1.7 \times 10^{-14}$	$<2.5 \times 10^{-15}$	10.12	0.000	0.920	I	Blob
587742575924805956	15:23:22.8	+13:26:19.2	15.91	1.38	3.4	2.8×10^{-14}	$<7.7 \times 10^{-15}$	9.99	0.000	0.038	I	Disturbed
587736477596975155	15:23:43.0	+08:27:29.0	15.86	2.06	3.0	$<5.2 \times 10^{-16}$	–	9.81	0.000	1.000	I	–
587739810494218509	15:24:25.6	+19:42:59.5	14.96	1.13	5.4	1.2×10^{-14}	$<1.4 \times 10^{-15}$	9.73	0.027	0.031	S	L; disturbed
587733603187556413	15:26:21.9	+48:42:14.4	15.88	1.58	3.9	1.4×10^{-13}	$<5.7 \times 10^{-14}$	10.07	0.310	1.000	I	–
588017703489634681	15:26:53.3	+08:32:07.7	16.64	2.21	4.7	$<1.3 \times 10^{-13}$	$<5.7 \times 10^{-15}$	10.00	0.000	0.359	I	Blob

Table 1 – continued

SDSS object ID (1)	RA (2)	Dec. (3)	m_r (4)	$u - r$ (5)	EW(H δ) (6)	$S_{[\text{O II}]}$ (7)	$S_{\text{H}\alpha}$ (8)	$\log(M_*)$ (9)	f_m (10)	fracDev (11)	Type (12)	Comment
587730021724062009	15:34:53.4	+04:16:60.0	15.66	1.43	3.5	1.9×10^{-15}	$<7.4 \times 10^{-16}$	10.00	0.000	0.181	I	Disturbed
587739721917595889	15:39:19.9	+21:21:30.0	16.76	2.05	3.1	$<3.9 \times 10^{-15}$	$<8.8 \times 10^{-16}$	9.86	0.000	1.000	I	Blob
588017704565276972	15:44:31.7	+08:35:07.4	16.52	1.93	3.6	$<6.4 \times 10^{-14}$	$<3.3 \times 10^{-15}$	9.75	0.000	0.717	S	–
588011101570662666	16:00:17.3	+46:51:35.6	16.57	2.28	3.3	$<9.8 \times 10^{-14}$	$<8.1 \times 10^{-15}$	10.29	0.000	0.779	E	Blob
587739828212793702	16:03:15.7	+16:19:07.9	15.86	2.09	3.6	3.1×10^{-14}	$<4.5 \times 10^{-15}$	10.07	0.044	0.814	I	Disturbed
587739809961804053	16:03:25.9	+15:38:48.2	15.43	0.84	4.0	5.7×10^{-14}	$<4.2 \times 10^{-15}$	9.55	0.000	0.106	S	L
587729227152752660	16:03:44.5	+52:24:12.6	15.57	2.23	4.3	$<5.8 \times 10^{-15}$	$<1.2 \times 10^{-15}$	10.42	0.000	1.000	E	–
587739707420901722	16:04:38.6	+17:36:35.0	16.61	2.00	3.8	$<3.3 \times 10^{-17}$	$<1.5 \times 10^{-16}$	9.46	0.186	0.499	I	Disturbed
587725817501712592	16:16:52.9	+50:57:04.6	14.69	2.73	4.0	–	$<6.7 \times 10^{-15}$	11.47	0.000	0.734	E	–
587735666928844900	16:25:18.3	+37:56:40.6	15.03	2.12	3.2	$<1.0 \times 10^{-15}$	$<1.6 \times 10^{-16}$	10.15	0.000	1.000	I	–
588018090548920817	16:41:33.5	+24:42:14.2	16.01	2.02	4.1	$<6.9 \times 10^{-15}$	$<2.3 \times 10^{-15}$	10.04	0.000	0.849	I	Blob
588018253228408956	16:53:14.4	+25:07:59.2	14.01	1.45	4.3	1.1×10^{-13}	$<9.3 \times 10^{-14}$	10.44	0.000	0.692	S	Disturbed
588018254302609790	16:59:33.1	+24:55:59.9	16.17	2.36	3.0	$<7.3 \times 10^{-16}$	$<2.2 \times 10^{-16}$	10.28	0.000	0.717	I	Blob
587733432998559923	17:04:51.3	+25:03:18.4	16.51	2.51	8.3	$<1.1 \times 10^{-14}$	$<2.4 \times 10^{-15}$	10.45	0.068	1.000	I	Blob
587725503947735340	17:14:07.2	+57:28:38.7	16.00	2.10	3.2	$<1.4 \times 10^{-14}$	$<8.2 \times 10^{-16}$	9.83	0.000	0.129	S	–
587731174382502294	21:19:48.2	+00:40:21.8	16.37	1.83	5.5	$<3.7 \times 10^{-16}$	$<5.5 \times 10^{-17}$	9.91	0.000	0.880	I	–
587727213347799419	21:33:56.5	–07:54:08.7	15.22	1.14	4.4	$<2.7 \times 10^{-16}$	$<5.5 \times 10^{-17}$	9.75	0.000	0.000	I	–
587731185117954089	22:08:06.1	–00:54:25.0	15.10	2.06	4.3	$<4.9 \times 10^{-16}$	$<3.3 \times 10^{-16}$	10.54	0.036	1.000	E	Disturbed

Columns. (1): SDSS object identification; (2): galaxy centre’s right ascension; (3): galaxy centre’s declination; (4): r -band magnitude; (5): $u - r$ colour; (6): H δ equivalent width (\AA); (7): measured [O II] flux densities in units of $10^{-17} \text{ erg s}^{-1} \text{ cm}^{-2} \text{ \AA}^{-1}$. The upper limits are defined to be four times the rms noise; (8): estimated upper limits for the H α flux densities in units of $10^{-17} \text{ erg s}^{-1} \text{ cm}^{-2} \text{ \AA}^{-1}$ as defined to be four times the rms noise; (9): log of the stellar masses obtained from Schawinski et al. (2007b) which were determined by fitting the five SDSS photometric bands to model star formation histories from Maraston (1998, 2005) stellar models; (10): weighted merger parameter (Darg et al. 2010); (11): the SDSS parameter which gives the fraction of light (in the r band) fitted by a de Vaucouleurs profile; (12): description of galaxy type where ‘S’ represents late-type spiral galaxies, ‘E’ represents early-type galaxies and ‘I’ represents intermediate-type galaxies; (10): comments from visual inspection of each galaxy. A ‘disturbed’ comment indicates that the stellar morphology appears to have been disrupted by tidal interaction with features such as stellar tails/rings or with neighbouring galaxies at close proximities. An ‘asymmetric’ comment defines an observed asymmetric stellar disc. An ‘–’ comment represents galaxies whose morphologies appear fairly regular, while a ‘blob’ comment refers to galaxy morphologies which are small, compact and fairly spherical in appearance. An ‘L’ comment indicates that this galaxy exhibits spectral signatures of a LINER.

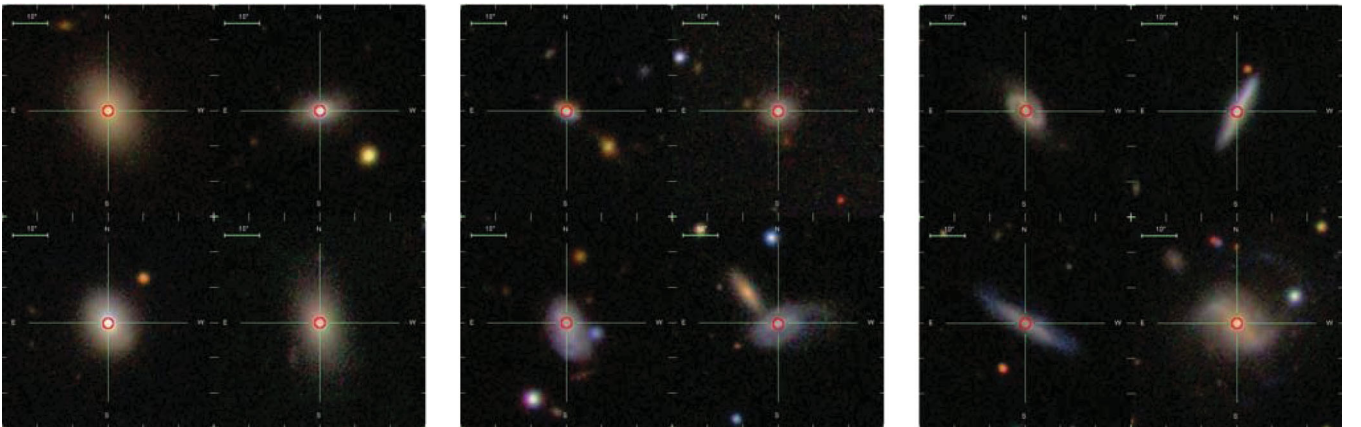


Figure 1. Example SDSS colour images of 12 PSGs within our sample. Each image frame provides a $48 \times 48 \text{ arcsec}^2$ field of view centred on the galaxy. The left-hand panel shows four examples of early-type PSGs, the middle panel shows four examples of intermediate-type PSGs and the right-hand panel shows four examples of late-type PSGs. The red circles show the SDSS fibre field of view where each spectrum was obtained.

3 RESULTS

3.1 Morphological properties

3.1.1 Morphological classification using Galaxy Zoo

Galaxy morphologies are derived from the Galaxy Zoo 1 project (Lintott et al. 2011). From the multiple independent inspections

(and classifications) made for each galaxy, the accuracy of the classifications for individual galaxies can be determined by imposing a required level of agreement among the classifiers. Following the definition of the CLEAN sample from Land et al. (2008), we require a minimum of an 80 per cent majority agreement on the morphology for each object. Spiral galaxies (from an Sa to an Sd morphology) are classified as *late-type* objects, while all spheroids (including lenticular galaxies) are classified as *early-type* objects.

Table 2. Distributions of galaxy morphologies and star formation properties of our entire local volume sample and that of the PSG sample. The distributions are listed as percentages and the numbers of galaxies are given in parentheses.

	Entire galaxy sample		Total	PSG sample
	Non-SF	SF		
Early type	50 per cent (5148)	10 per cent (3770)	19 per cent (8918)	16 per cent (13)
Intermediate	46 per cent (4841)	47 per cent (17 589)	47 per cent (22 430)	74 per cent (59)
Late type	4 per cent (388)	43 per cent (15 837)	34 per cent (16 225)	10 per cent (8)
Total	100 per cent (10 377)	100 per cent (37 196)	100 per cent (47 573)	100 per cent (80)

Galaxy morphologies that are neither ‘early type’ nor ‘late type’ are classified as *intermediate type*, which include galaxies with irregular/disturbed and merging morphologies.

Relative to the entire local volume sample, there is a smaller fraction of PSGs with spiral or late-type morphologies. We find that $74 (\pm 10)$ per cent of our PSG sample appear to have intermediate morphologies, while $16 (\pm 5)$ and $10 (\pm 4)$ per cent of our PSGs are classified as early and late types, respectively. It should be noted that a colour bias in morphology votes (by the Galaxy Zoo citizen scientists) is unlikely to occur since our PSG sample is dominated by intermediate-type morphologies. In addition, investigations by Lintott et al. (2008) found colour bias to not have a significant effect on the final morphological classifications.

Similar to the results of Baldry et al. (2004), Driver et al. (2006) and Bamford et al. (2009), we find that the majority of the spheroidal/elliptical galaxies within our local volume sample exhibit non-SF properties, while the SF galaxies tended to have spiral morphologies. In this paper, we classify a galaxy as SF if its H α emission line is stronger than four times the rms level. As expected from our PSG selection criteria of galaxies with recently truncated star formation, we find that the PSGs appear to have a morphology distribution which appears intermediate to that of SF and non-SF galaxies within the control sample. Table 2 lists the distribution of morphologies and SF properties of both the local volume control sample and the PSG sample.

In addition to the Galaxy Zoo classifications, we visually inspected each PSG to confirm the morphologies. Consistent with the fact that a majority of the PSGs have intermediate-type morphologies, we find disturbed galaxy morphologies which resemble neither early- nor late-type galaxies. Depending on the size of the galaxy, the 3 arcsec fibres (from which the SDSS spectra are obtained) may only correspond to the central 1.2–2.9 kpc of galaxies within our redshift range. In our sample, the observed spectral properties may not be representative for approximately 5 per cent of our sample where the outer galaxy regions are much greater than 3 arcsec and appear to be bluer than the central region.

The f_m parameter is a quantification of the merger properties of Galaxy Zoo 1 and is defined to be the weighted-merger-vote fraction where the fraction of merger votes is multiplied by a weighting factor (W ; Lintott et al. 2008) to account for the quality of the particular voters who have assessed each galaxy (Darg et al. 2010). Assuming that $f_m > 0.4$ describes a merger (Darg et al. 2010), we do not find many mergers within our PSG sample even though a large number of the PSGs appear asymmetrical or disturbed. A comparison of the distribution of f_m parameters of our PSG sample to those of the early and late types of the entire galaxy sample yields Kolmogorov–Smirnov (KS) probabilities which indicate that there are no significant differences between any of the f_m distributions. Fig. 2 shows the normalized cumulative distributions of f_m for the different galaxy types.

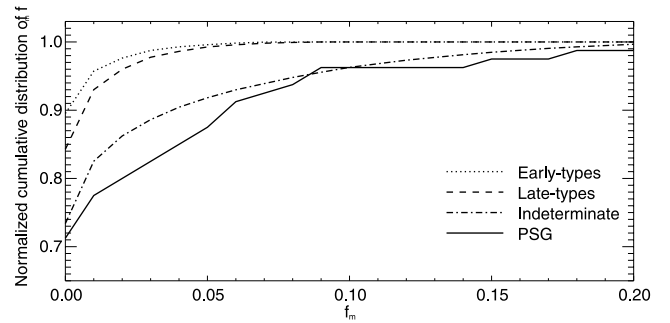


Figure 2. Peak-normalized cumulative distributions of f_m for our PSG sample (black solid line) and the different types of galaxies within the control sample.

3.1.2 Concentration

As the majority of our PSG sample consist of intermediate-type morphologies, further investigation of the stellar structure will reveal quantitatively whether these PSGs truly have intermediate-type morphologies (possibly due to past interactions) or are similar in structure to the early- or late-type galaxies within the same volume. We measure the concentration index using the ratio between the $R90$ and $R50$ parameters which are the radii where 90 and 50 per cent of the total Petrosian² flux have been measured in the i band. Therefore, bulge-dominated galaxies will have greater $R90/R50$ ratios, while disc-dominated galaxies will have smaller values.

To determine the end products of our PSG sample, we compare the peak-normalized distributions of concentration indices for our population of PSGs to the early- and late-type populations of galaxies with $\log(M_*) < 10.5 M_\odot$. In agreement with Strateva et al. (2001), we find that the division between early- and late-type galaxies is where $R90$ is approximately 2.6 times greater than $R50$. The distribution of concentration indices for our PSG sample is very similar to that of the early-type galaxies.

On the other hand, Masters et al. (2010) showed that early-type galaxies classified in such a manner may be contaminated by up to 50 per cent by edge-on spirals and that the SDSS fracDev parameter (which gives the fraction of light fitted by a de Vaucouleurs profile) provides a better differentiation between the early- and late-type galaxies as typical early-type elliptical galaxies are traditionally characterized by a de Vaucouleurs profile and as such have $\text{fracDev} > 0.5$. As such, we show the distribution of fracDev for our ‘green’ PSGs and low-mass early- and late-type samples in Fig. 3. The PSG distribution is shown by the grey-shaded histogram, while the striped histogram in the left-hand panel represents

² A Petrosian radius is where the mean local surface brightness (within the local annulus) is equal to a constant fraction of the mean surface brightness within that radius (Strauss et al. 2002).

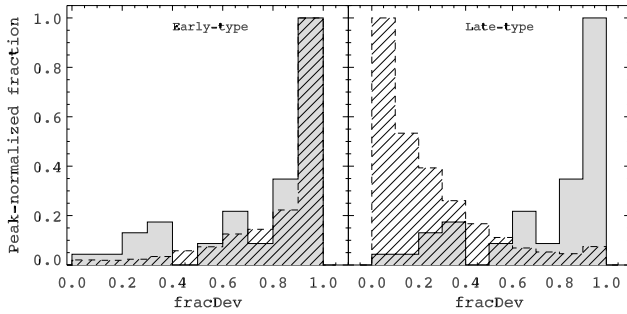


Figure 3. Peak-normalized distributions of fracDev (which describes the fraction of light from a fit to a de Vaucouleurs profile). The grey-shaded histograms show the fracDev distribution for PSGs. The striped histogram shows the fracDev distribution for the early-type galaxies (left-hand panel) and the fracDev distribution for the late-type galaxies (right-hand panel).

the distribution for the early types, and the distribution for late types is represented by the striped histogram in the right-hand panel. A quantitative comparison using the KS test yields a KS probability of 0.68 that the fracDev distributions of PSGs and early types are derived from the same parent sample, while the fracDev distributions of PSGs and late types yield a KS probability of <0.001 .

Therefore, we find that the structural stellar morphologies of the PSGs within the ‘green valley’ appear to be more closely related to the morphologies of low-mass early-type galaxies even though star formation has only been truncated recently.

3.2 Colour and stellar mass

We derive the $u - r$ colours of our sample using the `modelMag` values (from SDSS DR7; Abazajian et al. 2009) that are determined from the best fit of each galaxy profile to the linear combination

of the exponential and the de Vaucouleurs profiles. In addition, these magnitude measurements are corrected for dust attenuation using the models of Calzetti et al. (2000). The ‘green valley’ of our sample’s colour distribution is defined to be within the nominal colour range of $1.8 < u - r < 2.3$. The stellar mass estimates for each galaxy are measured by fitting the five optical wavebands from SDSS to star formation history libraries generated from stellar models of Maraston (1998, 2005). The uncertainties in our derived stellar masses are dominated by the inherent uncertainties within the stellar models used. More details on the parametrization of the star formation histories and the fitting process can be found in Schawinski et al. (2010) and references therein.

The top row of panels in Fig. 4 show the colour–stellar mass distribution of our PSG sample as the red solid circles and the SDSS galaxy sample of a particular type is represented by the black solid contours. The dotted-line contours represent the distribution of the entire sample regardless of galaxy type and are shown for comparison purposes. The bottom row of panels in Fig. 4 show the distribution of PSG fraction (of a particular type) in a given colour–stellar mass bin as the solid orange-shaded contour map overlaid on the solid contours showing the distribution of the SDSS galaxies of a particular type.

As can be seen from the top row panels of Fig. 4, our PSG sample appears to be spread over a fairly large $u - r$ colour range even though a majority (94 per cent) of the PSGs have stellar masses below the transition mass of $\log M_* < 10.5 M_\odot$ which separate the low-mass SF galaxies from the high-mass passively evolving bulge-dominated galaxies (Kauffmann et al. 2003). In fact, we do not find any PSG with $\log M_* > 11.5 M_\odot$. Such a stellar mass limit in our PSG sample is more clearly illustrated by the number fractions of PSGs to the number of galaxies within a particular colour–stellar mass range (see the bottom panels of Fig. 4). Fig. 5 shows the percentage of PSGs per $10^{0.5} M_\odot$ bin. The average percentage of

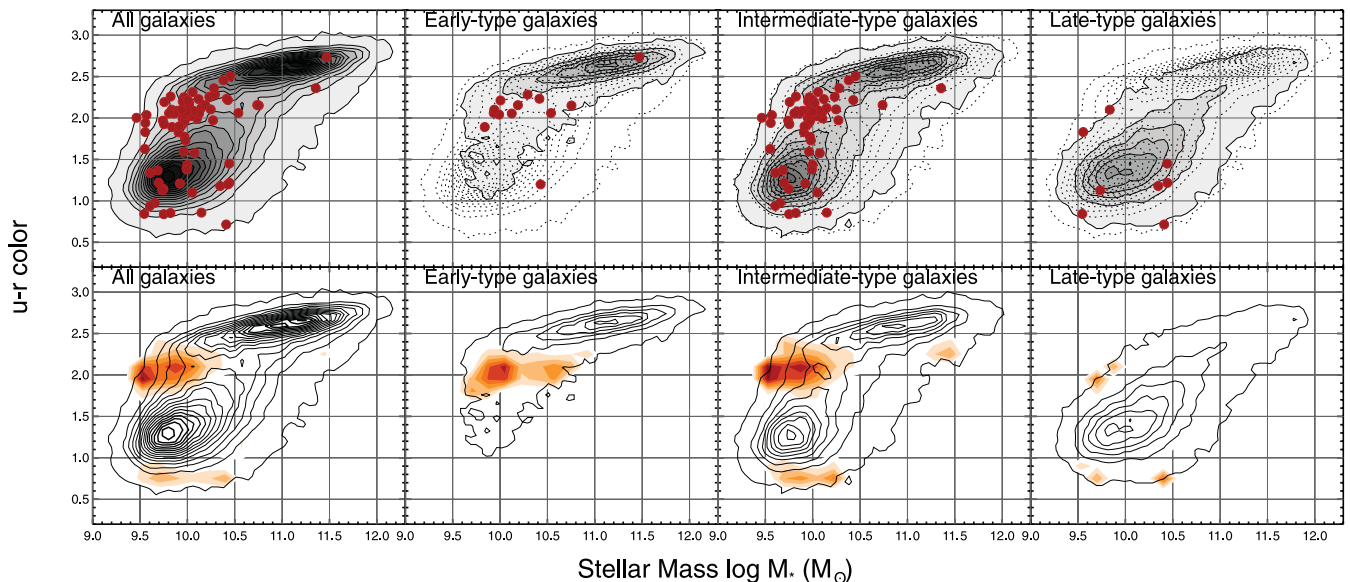


Figure 4. The $u - r$ colour versus stellar mass distributions of our SDSS galaxy sample are shown by the contours. The top row of panels show the PSG sample (solid red circles) overlotted on to the distribution of SDSS galaxies of a particular type (demarcated by the solid contours). The panels from the left-hand to right-hand side show the distributions: for all galaxy types, for early-type galaxies, for intermediate-type galaxies and for late-type galaxies. In the top row, the distributions of SDSS galaxies for all galaxy types are also shown, for comparison purposes, by the dotted contours in the early-, intermediate- and late-type galaxy panels. The bottom row of panels show the number fraction of our PSG sample to the galaxy sample of a particular type in a given colour–stellar mass bin as the solid orange-shaded contour map overlaid on to the contours marking the distribution of SDSS galaxies. The maximum number fractions for all galaxy types, early types, intermediate types and late types are 3.0, 2.6, 3.0 and 1.9 per cent, respectively.

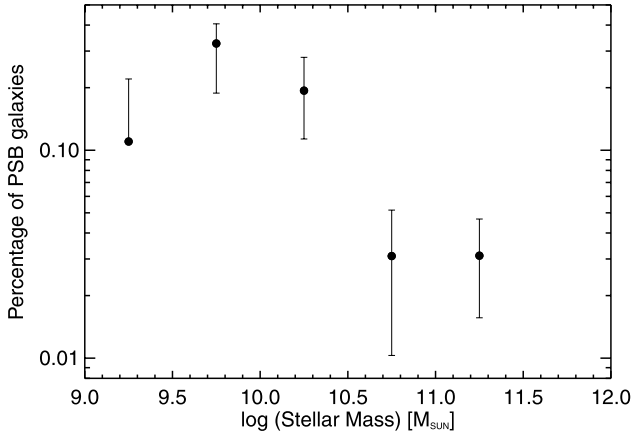


Figure 5. Percentage of PSBs as a function of stellar mass. The uncertainties are given by the 10th and 90th percentile values derived from bootstrap resampling of our data.

PSBs in the $\log M_*$ bins between 9.5 and $10.5 M_\odot$ is approximately eight times greater than that in the $\log M_*$ bins between 10.5 and $11.5 M_\odot$ (with a 3σ significance). The uncertainties in the stellar masses are dominated by the uncertainties in the stellar population models and can be up to $10^{0.3} M_\odot$ in stellar masses (e.g. Conroy, Gunn & White 2009).

One possible reason for the lack of high-mass PSBs is likely to be because our sample is restricted to a very local volume. As such, the probability of finding massive galaxies in such a local volume is much less than at higher redshifts. Galaxies with \log stellar masses greater than 11.5 account for only 3.8 per cent of the entire galaxy sample. In addition, high-redshift surveys of E+A galaxies are not as sensitive to smaller (and fainter) galaxies. As such, the E+A galaxies found at $z \sim 0.1$ are most likely the biggest and brightest types of PSBs. For example, the PSB sample at $z = 0.8$ in Yan et al. (2009) have stellar masses greater than $10^{10.6} M_\odot$. In addition, low-redshift PSBs are also more closely associated with less massive blue galaxies than high-redshift PSBs that are more similar to massive red galaxies (e.g. Yan et al. 2009). Therefore, it is not surprising that our local sample of PSBs is dominated by low-mass objects.

In addition to the apparent stellar mass limit of our PSB population, the bottom panels of Fig. 4 also show that a significant fraction (61 per cent) of our PSB sample reside within the ‘green valley’, while 31 and 8 per cent reside in the ‘blue cloud’ ($u - r < 1.8$) and the ‘red sequence’, respectively. Similarly, we find that the percentage of PSBs within the ‘green valley’ (0.6 per cent) is 17 and 6 times greater than the fraction of PSBs within the ‘red sequence’ and the ‘blue cloud’, respectively. Hence, we propose that local PSBs occupy a well-defined position in the low-mass end of the ‘green valley’. Recent observations of a smaller sample of K + A galaxies along the large-scale filamentary structures occurring at the ‘Great Wall’ allude to similar results (Gavazzi et al. 2010). Consistent with the idea of galaxy formation downsizing, we postulate that local PSBs will transform into passively evolving ‘red’ galaxies and contribute towards the build-up of the low-mass end of the ‘red sequence’ if star formation has indeed ceased.

3.3 Environment

Using the adaptive Gaussian environment parameter, ρ_g (which provides a measure of the number and proximity of galaxies around

Table 3. Fractions of galaxies in three different environment classes for different types of galaxies.

Galaxy type	$\rho_g < 0.21$	$0.21 < \rho_g < 0.58$	$\rho_g > 0.58$
Early type	45 per cent (4034)	29 per cent (2561)	26 per cent (2333)
Intermediate	53 per cent (11866)	27 per cent (6022)	20 per cent (4592)
Late type	56 per cent (9124)	28 per cent (4555)	16 per cent (2566)
PSG	50 per cent (40)	26 per cent (21)	24 per cent (19)

a point in space, see Schawinski et al. 2007a), we study the environment properties of our PSB sample. Low-, medium- and high-density environments are described by $\rho_g < 0.21$, $0.21 < \rho_g < 0.58$ and $\rho_g > 0.58$, respectively (Schawinski et al. 2007a). The low-density class of environment can be likened to the galaxy field environment. Similarly, the medium- and high-density classes can be compared to the group (or cluster outskirts) and cluster environments, respectively.

We find that 50 per cent of our sample reside in the low-density environment, while 26 and 24 per cent reside in the medium- and high-density environments, respectively. In high-density environments, the fraction of PSBs is similar to that of early types, while in low-density environments, the fraction of PSBs is in between that of intermediate- and early-type galaxies. As can be seen from Table 3, the number fractions of early- and late-type galaxies in the low- and high-density environments differ by ~ 10 per cent, whereby a greater fraction of early types are found in high-density environments and a greater fraction of late types are found in low-density environments. This greater fraction of early-type galaxies at higher densities recapitulates the well-known morphology–density relation found by Dressler (1980) and more recent studies such as Bamford et al. (2009). Similar to the PSB sample, the intermediate-type galaxies appear to have fractions that are in between those found for early and late types. In addition, the fractions of galaxies residing in medium-density environments are roughly the same regardless of galaxy types. It should be noted that KS tests comparing the ρ_g distributions of different galaxy types confirm these results. Hence, we find that the PSB distributions across all three environment classes are similar to those of the early- and intermediate-type galaxies. This is consistent with the fact that ~ 90 per cent of the PSB sample consists of galaxies classified as early- or intermediate-type galaxies. Our results are also consistent with those of Blake et al. (2004) who found that the local environments of E+A galaxies follow that of the general galaxy population.

4 DISCUSSION

Our results show that local PSBs represent one population of galaxies which currently occupy a well-defined position in the low stellar mass end of the ‘green valley’ and is rapidly transitioning on to the low-mass end of the ‘red sequence’ unless star formation resumes within the transitioning period of ~ 1 Gyr. The duration within which the individual PSB spends in the ‘green valley’ is probably only of the order of ~ 1 Gyr (the time-scale for the fading of the Lyman continuum from the current generation of young stars), because, structurally, the stellar concentration of the PSBs within the ‘green valley’ already closely resembles those of low-mass early-type galaxies even though star formation has only been truncated recently. Our transition time-scale concurs with recent findings of transition times of the order of ~ 1 Gyr between the ‘blue cloud’ and the ‘red sequence’ (e.g. Kaviraj et al. 2007, 2011; Schawinski et al. 2007b). These results are consistent with the idea of downsizing.

Previous galaxy evolution studies (e.g. Smail et al. 1998) alluded to the notion of downsizing by observing that the most luminous elliptical galaxies are formed at earlier epochs than less luminous early-type objects. Our results are therefore comparable to those of Wild et al. (2009) who found the mass density of PSGs to be 230 times lower at $z \sim 0.07$ than at $z \sim 0.7$.

Current galaxy evolution models often suggest that feedback from an AGN could provide the means to quench and truncate the star formation history of a massive galaxy (e.g. Silk & Rees 1998; Kaviraj et al. 2005; Croton et al. 2006). Incidentally, our observation of a stellar mass limit in our PSG sample coincides with the findings of Schawinski et al. (2010) who found that the AGN duty cycle peaks at the low-mass end of the ‘green valley’ and that the low-mass early-type AGN hosts appear to have post-starburst properties. However, apart from two PSGs which exhibit spectral properties of low-ionization nuclear emission-line regions (LINERs), we do not observe any spectral signatures of AGN within our PSG sample.

The connection between AGNs and mergers/interactions has been discussed in the context of mergers inducing inflows of gas that fuel star formation and the black hole (in the central regions; e.g. Canalizo et al. 2006), while feedback from AGNs is predicted to quench star formation by reheating the cold gas and expelling much of it in AGN-driven winds (e.g. Di Matteo, Springel & Hernquist 2005; Thacker, Scannapieco & Couchman 2006). Tremonti, Moustakas & Diamond-Stanic (2007) found evidence for these winds in 10 out of 14 PSGs at $z = 0.6$. They hypothesized that the observed gas outflows in these galaxies suggest that AGN feedback may play a role in quenching star formation in PSGs. Compared to the PSG sample of Tremonti et al. (2007), our local PSGs are redder and not as massive. Therefore, following the results of Yan et al. (2009) and Wild et al. (2009), we hypothesize that the evolution of our local PSG sample is likely to be different from that of PSGs at higher redshifts. Consistent with the results of Kaviraj et al. (2007), it is unlikely that AGN feedback will be a dominant quenching process for star formation in local PSGs.

5 SUMMARY

In this paper, we have presented a study of local PSGs using the photometric and spectroscopic observations from the SDSS in conjunction with the results from the Galaxy Zoo 1 project. We find the following:

(i) The local population of PSGs occupy a well-defined space in the colour–stellar mass diagram, most notably at the low-mass end of the green valley below the transition mass ($\log M_* < 10.5 M_\odot$; Kauffmann et al. 2003) thought to be the mass division between low-mass SF galaxies and high-mass passively evolving bulge-dominated galaxies. Consistent with the idea of galaxy formation downsizing where smaller galaxies form at later epochs, we think that the local PSGs will contribute to the build-up of the low-mass end of the red sequence if star formation has indeed ceased in these galaxies.

(ii) Consistent with previous studies (e.g. Blake et al. 2004), we find that the local environment of local PSGs follows that of the general galaxy population within the same volume.

(iii) Using the morphological classifications from Galaxy Zoo, we are able to study the distributions of morphologies in our PSG sample in comparison to those of 47 573 galaxies in our full galaxy sample within the same local volume. Although a majority of our local PSG sample appear to have intermediate-type morphologies that are neither early- nor late-type morphologies, we find the stel-

lar structural morphology (as described by `fracDev`) of the local ‘green valley’ PSGs to be very similar to that of low-mass early-type galaxies in the ‘red sequence’ even though star formation has only recently ceased. Therefore, unless star formation resumes, we hypothesize that the local PSGs will evolve out of the ‘green valley’ in ~ 1 Gyr on to the ‘red sequence’ as soon as the young stellar population from the most recent episode of star formation fade.

ACKNOWLEDGMENTS

Galaxy Zoo acknowledges support from The Leverhulme Trust. OIW is the recipient of a Super Science Fellowship from the Australian Research Council. Support for the work of KS was provided by NASA through Einstein Postdoctoral Fellowship grant number PF9-00069 issued by the Chandra X-ray Observatory Center, which is operated by the Smithsonian Astrophysical Observatory for and on behalf of NASA under contract NAS8-03060. KLM acknowledges funding from the Peter and Patricia Gruber Foundation as the 2008 Peter and Patricia Gruber Foundation International Astronomical Union Fellow, from a 2010 Leverhulme Trust Early Career Fellowship and from the University of Portsmouth and SEPnet (www.sepnet.ac.uk). The authors also thank the anonymous referee for the constructive comments which have improved this paper.

REFERENCES

- Abazajian K. N. et al., 2009, *ApJS*, 182, 543
 Abraham R. G. et al., 1996, *ApJ*, 471, 694
 Baldry I. K., Glazebrook K., Brinkmann J., Ivezić Ž., Lupton R. H., Nichol R. C., Szalay A. S., 2004, *ApJ*, 600, 681
 Baldry I. K., Balogh M. L., Bower R. G., Glazebrook K., Nichol R. C., Bamford S. P., Budavari T., 2006, *MNRAS*, 373, 469
 Balogh M. L., Morris S. L., Yee H. K. C., Carlberg R. G., Ellingson E., 1999, *ApJ*, 527, 54
 Bamford S. P. et al., 2009, *MNRAS*, 393, 1324
 Bekki K., Shioya Y., Couch W. J., 2001, *ApJ*, 547, L17
 Blake C. et al., 2004, *MNRAS*, 355, 713
 Caldwell N., Rose J. A., 1997, *AJ*, 113, 492
 Calzetti D., Armus L., Bohlin R. C., Kinney A. L., Koornneef J., Storchi-Bergmann T., 2000, *ApJ*, 533, 682
 Canalizo G., Stockton A., Brotherton M. S., Lacy M., 2006, *New Astron. Rev.*, 50, 650
 Conroy C., Gunn J. E., White M., 2009, *ApJ*, 699, 486
 Couch W. J., Sharples R. M., 1987, *MNRAS*, 229, 423
 Couch W. J., Ellis R. S., Sharples R. M., Smail I., 1994, *ApJ*, 430, 121
 Croton D. J. et al., 2006, *MNRAS*, 365, 11
 Darg D. W. et al., 2010, *MNRAS*, 401, 1043
 Di Matteo T., Springel V., Hernquist L., 2005, *Nat*, 433, 604
 Dressler A., 1980, *ApJ*, 236, 351
 Dressler A., Gunn J. E., 1983, *ApJ*, 270, 7
 Dressler A., Gunn J. E., 1992, *ApJS*, 78, 1
 Dressler A., Oemler A., Jr, Butcher H. R., Gunn J. E., 1994, *ApJ*, 430, 107
 Dressler A., Smail I., Poggianti B. M., Butcher H., Couch W. J., Ellis R. S., Oemler A., Jr, 1999, *ApJS*, 122, 51
 Dressler A., Oemler A., Jr, Poggianti B. M., Smail I., Trager S., Shectman S. A., Couch W. J., Ellis R. S., 2004, *ApJ*, 617, 867
 Driver S. P. et al., 2006, *MNRAS*, 368, 414
 Drory N. et al., 2009, *ApJ*, 707, 1595
 Fabricant D. G., McClintock J. E., Bautz M. W., 1991, *ApJ*, 381, 33
 Gavazzi G., Fumagalli M., Cucciati O., Boselli A., 2010, *A&A*, 517, 73
 Goto T., 2004, *A&A*, 427, 125
 Goto T., 2005, *MNRAS*, 357, 937
 Goto T., 2007, *MNRAS*, 381, 187
 Goto T. et al., 2003, *PASJ*, 55, 757
 Hunter D. A., 1994, *AJ*, 107, 565

- Hunter D. A., Gallagher J. S., III, 1990, *ApJ*, 362, 480
 Kannappan S. J., Guie J. M., Baker A. J., 2009, *AJ*, 138, 579
 Kauffmann G. et al., 2003, *MNRAS*, 341, 54
 Kauffmann G., White S. D. M., Heckman T. M., Ménard B., Brinchmann J., Charlot S., Tremonti C., Brinkmann J., 2004, *MNRAS*, 353, 713
 Kaviraj S., Devriendt J. E. G., Ferreras I., Yi S. K., 2005, *MNRAS*, 360, 60
 Kaviraj S., Kirkby L. A., Silk J., Sarzi M., 2007, *MNRAS*, 382, 960
 Kaviraj S., Schawinski K., Silk J., Shabala S. S., 2011, *MNRAS*, 936
 Kennicutt R. C., Jr, 1992, *ApJ*, 388, 310
 Kennicutt R. C., Jr, 1998, *ARA&A*, 36, 189
 Land K. et al., 2008, *MNRAS*, 388, 1686
 Lintott C. J. et al., 2008, *MNRAS*, 389, 1179
 Lintott C. et al., 2011, *MNRAS*, 410, 166
 MacLaren I., Ellis R. S., Couch W. J., 1988, *MNRAS*, 230, 249
 Maraston C., 1998, *MNRAS*, 300, 872
 Maraston C., 2005, *MNRAS*, 362, 799
 Martin C. L., 1998, *ApJ*, 506, 222
 Martin D. C. et al., 2007, *ApJS*, 173, 415
 Masters K. L. et al., 2010, *MNRAS*, 404, 792
 Newberry M. V., Boroson T. A., Kirshner R. P., 1990, *ApJ*, 350, 585
 Poggianti B. M., Smail I., Dressler A., Couch W. J., Barger A. J., Butcher H., Ellis R. S., Oemler A., Jr, 1999, *ApJ*, 518, 576
 Sarzi M. et al., 2006, *MNRAS*, 366, 1151
 Schawinski K. et al., 2007a, *ApJS*, 173, 512
 Schawinski K., Thomas D., Sarzi M., Maraston C., Kaviraj S., Joo S., Yi S. K., Silk J., 2007b, *MNRAS*, 382, 1415
 Schawinski K. et al., 2010, *ApJ*, 711, 284
 Silk J., Rees M. J., 1998, *A&A*, 331, L1
 Smail I., Edge A. C., Ellis R. S., Blandford R. D., 1998, *MNRAS*, 293, 124
 Strateva I. et al., 2001, *AJ*, 122, 1861
 Strauss M. A. et al., 2002, *AJ*, 124, 1810
 Thacker R. J., Scannapieco E., Couchman H. M. P., 2006, *ApJ*, 653, 86
 Tran K., Franx M., Illingworth G. D., van Dokkum P., Kelson D. D., Magee D., 2004, *ApJ*, 609, 683
 Tremonti C. A., Moustakas J., Diamond-Stanic A. M., 2007, *ApJ*, 663, L77
 Wei L. H., Kannappan S. J., Vogel S. N., Baker A. J., 2010, *ApJ*, 708, 841
 Wild V., Walcher C. J., Johansson P. H., Tresse L., Charlot S., Pollo A., Le Fèvre O., de Ravel L., 2009, *MNRAS*, 395, 144
 Yamauchi C., Yagi M., Goto T., 2008, *MNRAS*, 390, 383
 Yan R. et al., 2009, *MNRAS*, 398, 735
 Yang Y., Zabludoff A. I., Zaritsky D., Mihos J. C., 2008, *ApJ*, 688, 945
 York D. G. et al., 2000, *AJ*, 120, 1579

This paper has been typeset from a $\text{\TeX}/\text{\LaTeX}$ file prepared by the author.